This is a non peer-reviewed preprint, currently under consideration at Nature Geoscience

Deformation controlled Long-Period seismicity in low cohesion volcanic sediments

Pete Rowley[1,2], Philip P Benson[1], Christopher J Bean[3]

[1] Rock Mechanics Laboratory, School of Earth and Environmental Sciences, University of Portsmouth, Portsmouth, PO1 3QL, UK peter.rowley@uwe.ac.uk

[2] Department of Geography and Environmental Management, Frenchay Campus, UWE, Bristol, Coldharbour Lane, Bristol BS16 1QY, UK, philip.benson@portsmouth.ac.uk

[3] Geophysics Section, Dublin Institute for Advanced Studies, School of Cosmic Physics, 5 Merrion Square, Dublin 2, Ireland, chris.bean@dias.ie

Abstract

Volcano seismicity is an important tool in remotely monitoring and forecasting activity at volcanoes around the world. Volcanic earthquakes show diverse spectral characteristics, with shallow Long Period (Low Frequency) seismicity and long duration tremor generally interpreted as indicators of fluid migration, and as potential precursors to eruption. Here we show that a common low-cohesion volcanic sediment from Campi Flegrei caldera (Italy) produces Low Frequency and long duration seismicity whilst undergoing deformation in dry conditions. We employ acoustic-emission rock deformation experiments at a range of strain rates to produce events which are spectrally indistinguishable when normalised for scale from Long Period and tremor seismicity observed in natural volcanic settings. Generation of these signals is enhanced at lower strain rates. Correlated X-Ray tomography of samples before and after deformation constrain the source as distributed damage.

Given the ubiquitous nature of slow edifice deformation, and the frequent occurrence of such low cohesion materials in the upper edifice of volcanoes, we suggest low frequency seismicity and tremor in volcanic settings do not require fluid movement. Instead, these characteristic signals can be an indicator that deformation within the edifice is being accommodated by weak volcaniclastic materials.

Introduction

Volcano seismic monitoring is a key component of hazard management at volcanic centres around the world, enabling centralized observatory staff to monitor otherwise remote volcanoes. This is important as the increase in event-rate and character of seismic activity is strongly correlated with increasing volcanic rest and ultimately to eruption[1–3]. However, any hazard warning process is dependent on the quality of data gathered, and on the interpretation of that data in understanding volcanic processes.

A number of diagnostic volcanoseismic signals have identified as occurring within the near-surface volcanic edifice[4] , and are used in forecasting the eruption potential of active volcanoes. Long period (LP) and seismic tremor events are thought to be a result of fluid oscillation or movement within the volcanic edifice[2,5,6], and are characterized by long trains of low frequency signals lasting seconds (LP) to days (tremor). They often have no clear onset which makes 3D location difficult. Volcano-tectonic (VT) events are rapid-onset broad spectrum events, associated with rock fracture, as with tectonic events[7]. Hybrid earthquakes display the rapid and high frequency onset of VT events, with a subsequent low frequency train similar to LP events, and are usually interpreted as a combination of new fracture formation followed by fluid movement[8].

Of these, LP events and seismic tremor have been used as key early warning indicators, as the inference that fluid is moving may indicate either magma progression through the edifice, or movement of newly heated groundwater. However, despite the desire of scientists to use the fluid-related data to better forecast unrest, this has proved difficult. An improved understanding of the cause of these signals would enable better interpretation of seismic monitoring for improved hazard assessment, as false alarm evacuations can have disproportionate socioeconomic impacts on communities[9–13], while missed evacuations may directly result in unnecessary fatalities[14]. An increasingly recognised issue is that volcanic areas consist of a wide variety rocks, spanning from competent lavas to poorly consolidated ash and pumice. These latter rock type scatter and corrupt seismic energy in ways that are not fully understood from a rock physics perspective[15,16].

To better understand these LF and seismic tremor data, we here report a laboratory study using Neapolitan Yellow Tuff (NYT), as a representative example of the types of a weak volcaniclastic sediment often found within volcanic architectures. The NYT is a 40 km^3, often massive lapilli tuff, erupted from Campi Flegrei 14.9±0.4 ka[13,17,18], and therefore also forms part of the sedimentary cover involved in ongoing volcanic deformation in the area[19–21]. Produced during what is believed to be a phraeatomagmatic eruption, it is rich in pumice and pumiceous ash, with some lithics, and occasional accretionary lapilli[22]. The tuff as a whole is greater than 80 m thick in places, with the deposits showing intermittent dune bedforms and cross stratification as well as the more typical massive form. Its strength is low enough to be broadly representative of weakly lithified volcanic sediments in the upper edifice of active volcanoes around the world[23–25].

To better understand fluid-rock processes in the volcanic plumbing system, which may not be easily accessed in the field, considerable effort has been made to develop laboratory experiments with which to simulate volcano-tectonic pressures[26] and temperatures[27]. By combining high pore pressure fluid (and fluid movement) with freshly faulted rock samples, the seismic signature of the coupled rock-fluid has been simulated. The analogue of tectonic earthquakes is recorded on the cm-scale using and array of Acoustic Emission (AE) sensors, which have a relatively flat response across 100-800 kHz to capture seismicity at the laboratory scale[5,28]. Importantly, the physics of fracture and seismicity follows classical Boltzmann statistics allowing event sequences and character to be considered scale invariant, and allowing the AE at micrometre scale to be robustly applied to seismicity at kilometre scale[29,30]. Recent work has shown that the ratio of the scale of the feature (fault, conduit) to the seismicity follow a constant[5,31,32], and have successfully been used to model seismic processes in volcanic settings[33,34].

Mechanical behaviour

The NYT is a weak material, and – for the blocks used in this work – we find unconfined compressive strength (UCS) of dried samples in the range of 6-8MPa (consistent with previous work[35]). This places it at the weaker end of volcaniclastic sediments which have been tested[25]. We measure a cohesion of 0.18 MPa, comparable with that of medium clays, but far lower than that of either typical crystalline volcanic rocks (e.g. Columbia Plateau Basalt, 1-4 MPa) or more lithified ignimbrite material (Calico Hills tuff, 1.7-4.4 MPa). We therefore consider that the NYT is an appropriate analogue for the weak volcaniclastic sediments found in the upper edifice of volcanoes, while retaining the competence necessary to undergo coring and testing.

The nature of deformation during these experiments is dependent on strain rate. High strain rate conditions generate noticeable fractures running through the sample, with lengths on the order of centimetres, while low strain rate deformation results in shortening with no evidence of macroscopic fracture. This observation is supported by the use of X-ray computed tomography (XCT) analysis of the cores before and after deformation. Comparing virtual slices of the pre-and post-deformation cores reveals no visible fracturing or localised deformation at the resolution of the imaging (Figure 1). Given the 2% shortening of each sample during deformation this indicates that the damage was diffuse. Given the XCT resolution of 20 µm and the lack of individual damage zones, we are restricted to saying that the length scale of motion for individual AE events is no more than this resolution, and quite likely substantially smaller.

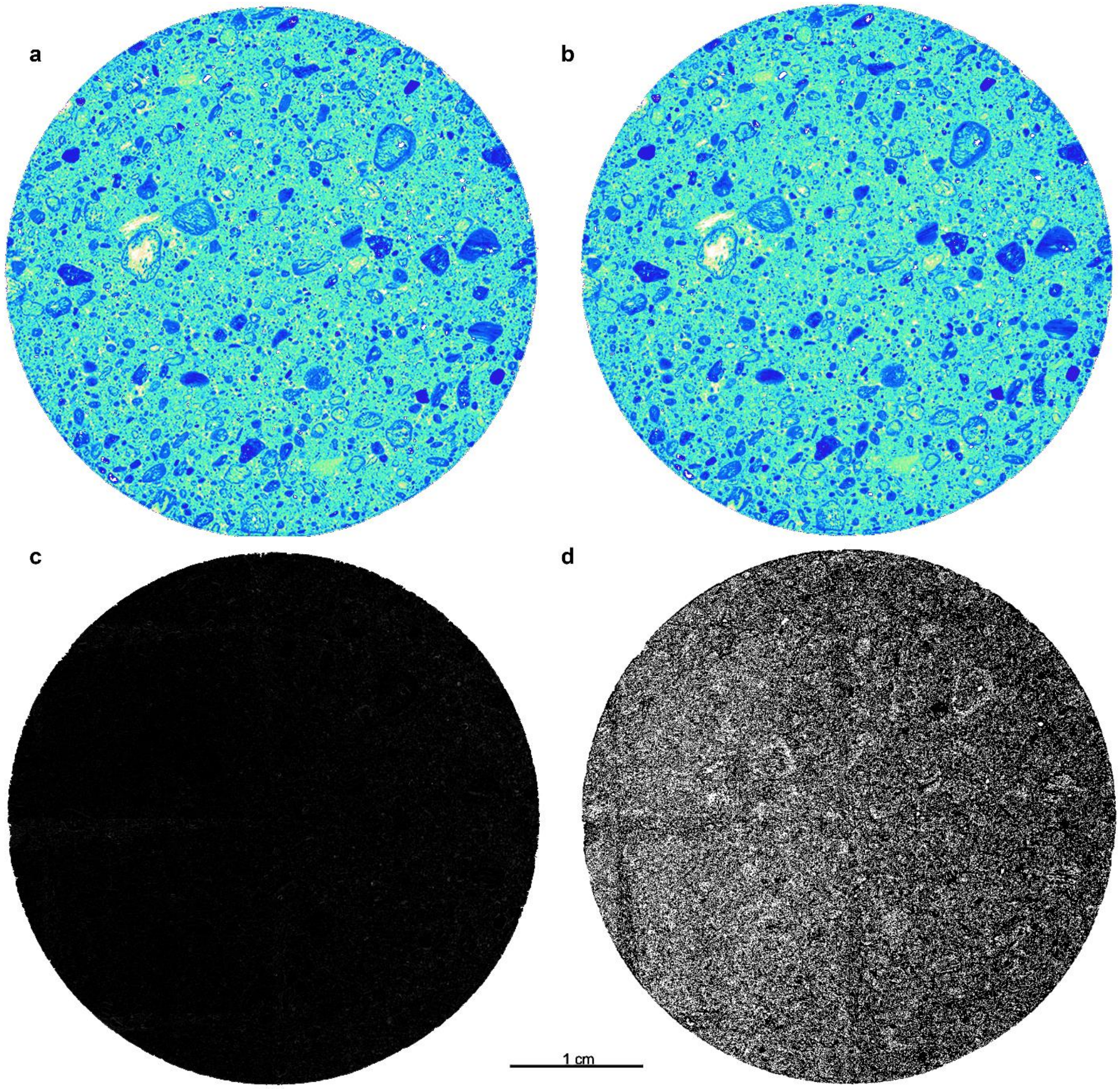

Figure 1. Example X-Ray computed tomography virtual slices of a sample before and after a low strain rate deformation experiment. **a** False-coloured section before testing, and **b** matched location after testing. **c** A comparison between pixel values in slices a and b, with bright pixels representing more difference on a grayscale range from 0 (black) to 255 (white). The dark colour indicates a broadly unchanged pixel character across the entire slice. **d** A high contrast version of c, stretching the grayscale across only the lowest 8 values. This threshold analysis shows that what little difference is present is localised around grain boundaries. This difference approach will preferentially highlight boundaries between material types, suggesting the deformation is even more diffuse than this analysis indicates. At this level of exaggeration weak linear artefacts are visible running vertically and horizontally across the image as a result of the XCT imaging process.

On the macro-scale, it is notable that there is no obvious ‘barrelling’ of the samples, whereby axial shortening is accompanied by lateral extension due to cataclasis and flow in the materials, as is common in lower porosity materials. The exceptionally high porosity and therefore space accommodation potential of the material is likely to account for this lack of radial strain in the samples. Post-experiment, all specimens were recovered from the rubber jacket without collapsing, maintaining structural integrity. This mode of failure is similar to that seen in compaction bands[36], rather than a propagating brittle failure via shear zones as commonly generated in competent (strong) rocks[37].

Spectral character of microseismicity in the Neapolitan Yellow Tuff

Acoustic emission was recorded during deformation of each sample in order to characterise the seismic behaviour under different conditions. Experiments using oven-dried samples, under both high and low strain rates ($1x10^{-5}$ s^{-1} & $4x10^{-6}$ s^{-1} respectively), produced spectra with dominant frequencies in the ranges 100 kHz to 150 kHz, and bimodal split across peaks at 150kHz and 600kHz. These are qualitatively very similar to the spectral features of volcanic LP, tremor, and hybrid type signals (Figure 2). Fracture propagation in competent, high cohesion rocks[33,38–40] is usually dominated by broad spectrum, short duration (10^{-5} s) events with spectral similarity to classic tectonic and volcano-tectonic (VT) seismic signatures (spectra covering the 200-800 kHz band and durations of <10^{-5} s, e.g. Fig 2a), as reported from deformation of basalt[33,34,41]. It is therefore notable that the NYT is almost completely dominated by activity in the low frequency (0-350 kHz) band, with durations into 10^{-4} and 10^{-3} s. Moreover, whilst LP data has been postulated to rely on fluid movement driving conduit/crack resonance to generate a lower frequency harmonic[5,42], here the samples are dry and so this generation mechanism is not available.

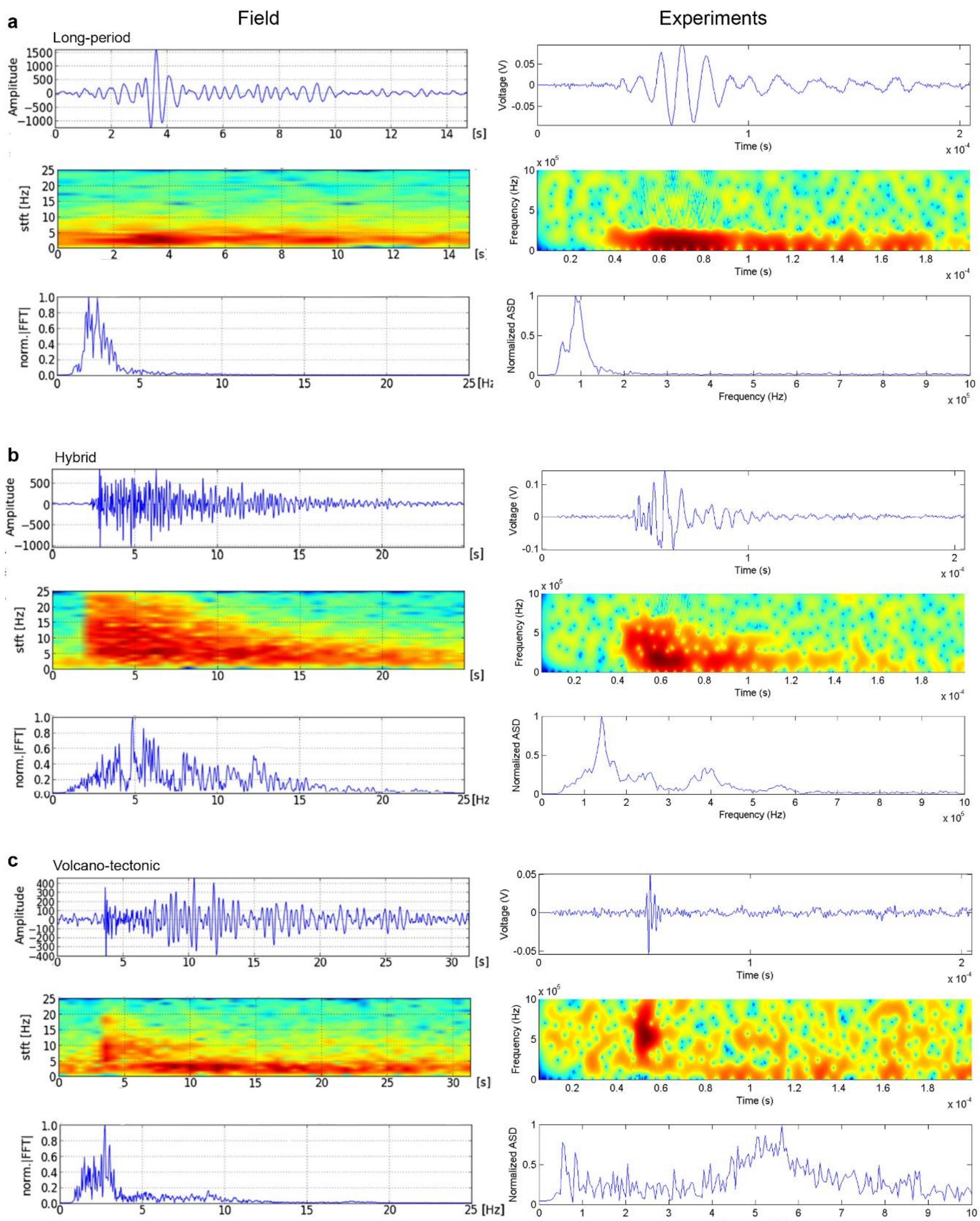

Figure 2 - Event representations of typical natural volcanic events[4] and typical experimental events recorded in this work, representing **a** long period (LP), **b** hybrid and **c** volcano tectonic (VT) style seismicity. Each event shows the vertical component of the velocity seismogram (or voltage for the experimental equivalent, which is proportional to magnitude of compression), Fourier spectrogram, and normalized Fourier transform.

The different event types have particular spectral characters; The LP/ tremor-like events (Fig 2a) show peak amplitudes at between 50 and 150 kHz with narrow spectra containing little signal above 400 kHz. These signals can have durations exceeding 1×10^{-3} s. Hybrid events (Figure 1b) have a broad-band initial response, between 50 and 700 kHz, which gradually and sequentially loses the higher frequency components until the signal dies out completely, after approximately 1×10^{-4} s. The VT-like events (Figure 2c) have a broad band emission across the sensor range (50 kHz – 800 kHz), although often with an emphasised peak amplitude between 400-700 kHz. They have durations in the realm of 1×10^{-5} s. Note that real field events can look more complex in detail, often due to wave scattering at heterogeneous edifice structures.

Strain-rate dependent emission character

We explore the low frequency dominance in these experiments using average peak FFT, extracted from the continuously logged 10 MHz data stream (Figure 3). High strain rate experiments have a different AE behaviour to slow strain rate conditions. The brittle failure at high strain rates is accompanied by accelerating AE (Figure 3a), including VT, LP and hybrid-like signals. This continues throughout the ~10 minute window as the differential stress climbs from zero, through the elastic-deformation phase, to the peak strength of the material. However, after the sample passes its peak strength and deformation goes into strain-weakening behaviour the AE stops. We interpret this as a localisation of deformation along the coherent fracture planes which have formed, lubricated by gouge.

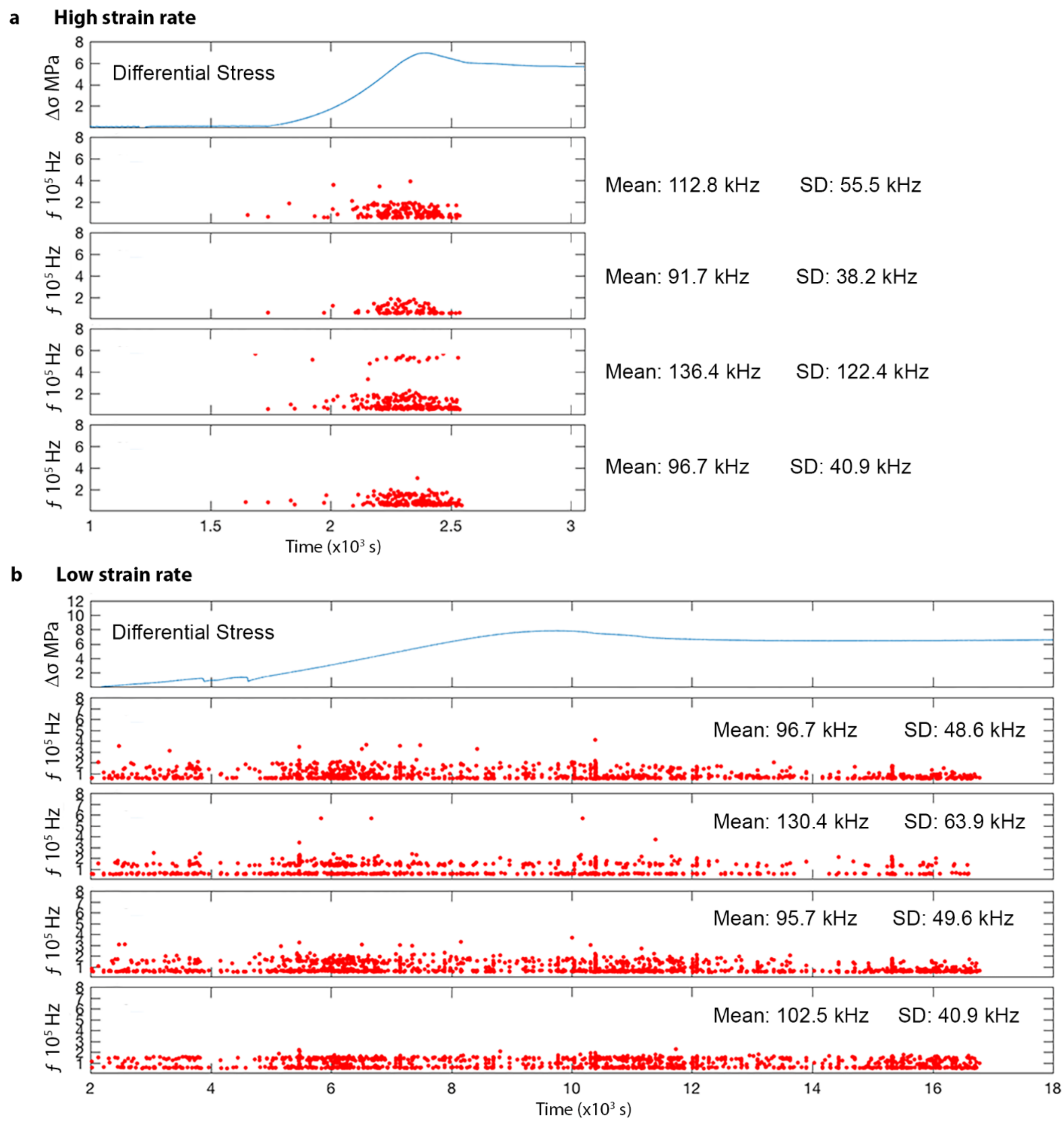

Figure 3 - Differential stress and moving average peak FFT frequency through time for 4 of the 12 AE channels in **a** high strain rate and **b** low strain rate experimental conditions. Note different horizontal scales. High strain rate experiments show accelerating AE until brittle failure of the sample. Low strain rate experiments show continuous activity throughout deformation.

In contrast, the low strain rate experiment (Fig 3b) begins exhibiting relatively consistent ‘tremor-like’ AE from the start of deformation, and throughout the experiment for over 5 hours, with evidence of slightly more activity in the first half of the elastic deformation phase, and in the strain weakening phase before the material behaves in a ductile manner. FFT analysis of these events allows moving average peak amplitude frequencies to be extracted, which give values of 119 kHz for the fast condition (σ 16.0 kHz) and 102 kHz for the slow strain rate condition (σ 15.3 kHz). This suggests that while both experiments are being dominated by low frequency LP and tremor-like signals the faster strain rate has a higher proportion of higher frequency VT- and hybrid-like signals. This is consistent with samples of individual event spectrograms generated for each experiment, which suggest in high strain rate experiments that ~7.5% of the signals are hybrid-like, and ~1% VT-like, whereas in low strain rate conditions under 1% of the AE are either VT- or hybrid-like. The remaining events are constrained entirely in the low frequency band (<350 kHz).

Generation of low frequency signal

While the LP- and tremor-like signals have very characteristic spectra, and they can be observed exhibiting durations two orders of magnitude longer than the VT-like events, there is a notable recurrence of events with similar durations to VT events but constrained to the LP- and tremor-like frequency band. High resolution AE spectrograms (Figure 4) suggest that many LP- and tremor-like signals may in fact be comprised of individual short-duration or overlapping events, sometimes exhibiting long trains of decreasing amplitude, sometimes with no clear train, and others with the trains punctuated by new peaks in activity at the same frequency.

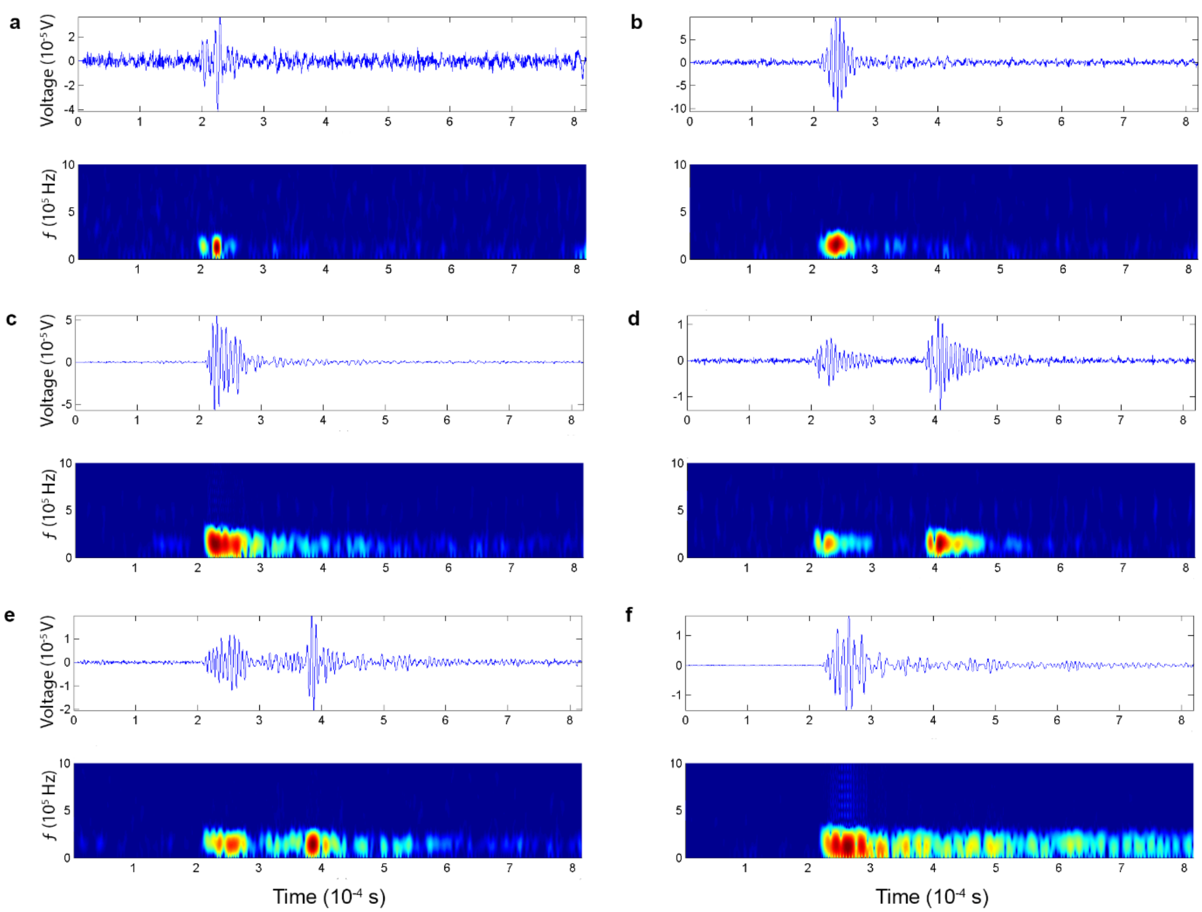

Figure 4 – **a-f** varied LP-type activity, which can be single or multiple pulse, with event timescales varying from 1 × 10^{-5} s to 1 × 10^{-3} s.

This rich behaviour seen in the experimental data shows a good qualitative match with field observations. The short duration pulses seen throughout the signals in Figure 4 bear similarity to pulse-like LP events[43], and to the often observed close relationship between LP and tremor, where rapidly repeating LPs have been seen to merge into longer duration tremor signals[44]. The detail of this character is seen in Figure 4f, where short duration LP events are embedded within low amplitude continuous tremor-like signals.

Discussion

Low cohesion volcaniclastic sediment has a substantially different acoustic emission behaviour to more common geomaterials which have been investigated in the laboratory to date, with a predominance of low frequency, long duration events. The propensity for the NYT to generate LP-like signals dominates the spectral characteristics regardless of strain rate under the conditions tested. Whilst VT-like events do occur, they represent a minority of the signal, as demonstrated by the mean FFTs (Figure 3).

Earthquake dominant frequencies scale with source dimension[31], so we use the established approach[32] $d_1 \times f_1 = d_2 \times f_2$ where *d* and *f* are the dimension and frequency of the events in the experiments (1) and the field (2) to explore the agreement between field and experiment. Spectral data for f1 and f2 (Figure 2) gives values for f_2/f_1 in the order of 10^5. Using XCT to assess damage in the tested material we find that d_1 has values *less than* 2×10^{-5} m, with this being a maximum value limited by the resolution of the XCT (Figure 1). This limits the length of rupture deformation in the field to <1 m, emitting at ~1 Hz). More likely, the deformation we see in the core is being accommodated by damage at smaller scales below the XCT resolution, bringing the associated anticipated deformation at volcanoes into the cm-scale seen commonly in active volcanic systems[45].

It has been suggested that shallow LP signals, and by inference, seismic tremor, may be generated by slow-failure in low strength materials[43]. The experiments here support the interpretation that deformation in dry materials can generate these signals. Using cross-correlated XCT images, we have, for the first time, been able to infer sub-grain scale distributed intergranular deformation of low cohesion sediments, linked to low frequency sustained acoustic emission. This suggests that LP seismicity may be generated distributed damage in low-cohesion materials accompanying edifice deformation.

Furthermore, these results suggest that deformation within weak porous volcanic materials may trigger similar signals to tremor and LP seismicity at low confining pressures, but without the presence or interaction of fluids. Given the frequent observation of shallow ground deformation in volcanic settings, it seems likely the conditions for subjecting volcanic sediments to these types of conditions are widespread. We do not suggest that tremor and LP signals cannot be produced by hydrothermal fluid and magma migration, but we highlight a mechanism for shallow seismicity and tremor unrelated to magma movement, with the capacity to confound the current interpretation of volcanic LP seismicity as always fluid-derived.

Method

The Neapolitan Yellow Tuff (Campi Flegrei, Italy) was collected from the Liccarblock quarry (40°53'29.42"N, 14° 6'25.74"E). Its physical characteristics were constrained using a range of uniaxial, triaxial shear tests, helium pycnometry, and thin section petrography. The NYT is a well-studied rock, not least because of its extensive use as a building stone in the Naples area. Typical of ignimbrite, it is spatially quite variable[17,46,47]. The deposit is up to ~80 m thick, and includes lenses which can be lithic-rich, pumice-rich, or accretionary lapilli-rich. The blocks used in this testing are relatively lithic poor, lack accretionary lapilli, and are characterised as a massive lapilli tuff.

Deformation experiments were carried out using a conventional triaxial testing machine[48] at a confining pressure of 1.5 MPa, simulating depths of 100 – 150 m. Cylindrical samples of 40 mm diameter and 100 mm length are encased in a rubber jacket fitted with ports for AE sensors. The jacket housing the 12 AE sensors also serves to separate the sample from the confining medium (silicone oil). To permit adequate control at low stress, conventional mechanical feedback was bypassed and instead a constant flow rate to the top piston/intensifier was used to ensure application of constant strain rate to the sample.

A digital logging system captured continuous signal date from all 12 AE sensors during the experiment at 10 MHz. These are first pre-amplified by 60dB, and passed through a hardware 1MHz low-pass filter. These data were subsequently harvested using a 50 mV threshold to identify individual events for spectral analysis.

Two different strain rates were tested; $1x10^{-5}$, and $4x10^{-6}$ s^{-1}, in an attempt to explore any strain dependent control of the spectral characteristics of any AE. These values were chosen based on the International Society for Rock Mechanics recommend strain rates in the order of 10^{-5} for simple unconfined compressive strength testing of rock samples to brittle failure, and 10^{-6} for complete stress-strain curves[49]. This ensures that this work is both comparable to other tests in the literature, and explores an order of magnitude strain rate variation.

X-ray Computed Tomography was carried out using a Zeiss Versa 510 X-ray microscope, achieving voxel resolutions within the samples of 20 µm. The cores were imaged both before and after the deformation experiments. The tomographic models were first viewed in an imaging software, and examined for damage. For direct comparison (e.g. Figure 1) a random slice was selected from the middle portion of the core in the pre-test tomographic model. Key identifying features were mapped, and then located in the post-experiment tomographic model. The model was manipulated until a virtual slice matching the same location in the pre-test was found in the post-test image.

Acknowledgements

We are grateful to Emily Butcher for sample preparation work, and to Emily Pegge for collating event classifications.

Competing Interests

The authors declare no competing interests.

Author Contributions

PR drafted the paper. PR & PB carried out the laboratory experiments. PR, PB, and CB discussed results, carried out analysis, and edited the draft paper.

References

1. Scarpa, R., Tilling, R. I. & McNutt, S. R. Seismic Monitoring and Eruption Forecasting of Volcanoes: A Review of the State-of-the-Art and Case Histories. in *Monitoring and Mitigation of Volcano Hazards* (1996). doi:10.1007/978-3-642-80087-0_3.

2. Chouet, B. A. Long-period volcano seismicity: Its source and use in eruption forecasting. *Nature* (1996) doi:10.1038/380309a0.

3. Kilburn, C. R. J. Multiscale fracturing as a key to forecasting volcanic eruptions. *J. Volcanol. Geotherm. Res.* **125**, 271–289 (2003).

4. Cortés, G. *et al.* Parallel System Architecture (PSA): An efficient approach for automatic recognition of volcano-seismic events. *J. Volcanol. Geotherm. Res.* **271**, 1–10 (2014).

5. Benson, P., Vincinguerra, S., Nasseri, M. H. B. & Young, R. P. Transition of low-frequency to very-low frequency volcano seismicity : New experimental insights. (2008).

6. Lokmer, I., Saccorotti, G., Di Lieto, B. & Bean, C. J. Temporal evolution of long-period seismicity at Etna Volcano, Italy, and its relationships with the 2004-2005 eruption. *Earth Planet. Sci. Lett.* **266**, 205–220 (2008).

7. McNutt, S. R. Seismic Monitoring and Eruption Forecasting of Volcanoes: A Review of the State-of-the-Art and Case Histories. in *Monitoring and Mitigation of Volcano Hazards* (eds. Scarpa, R., Tilling, R. I. & McNutt, S. R.) 99–146 (Springer, 1996). doi:10.1007/978-3-642-80087-0_3.

8. Harrington, R. M. & Benson, P. M. Analysis of laboratory simulations of volcanic hybrid earthquakes using empirical Green's functions. *J. Geophys. Res. Solid Earth* **116**, 1–13 (2011).

9. Barberi, F., Corrado, G., Innocenti, F. & Luongo, G. Phlegraean Fields 1982-1984: Brief chronicle of a volcano emergency in a densely populated area. *Bull. Volcanol.* (1984) doi:10.1007/BF01961547.

10. Armienti, P., Barberi, F. & Innocenti, F. A model of the Phlegraean Fields magma chamber in the last 10,500 years. *Bull. Volcanol.* (1984) doi:10.1007/BF01961566.

11. Scarpa, R., Tilling, R. I., Barberi, F. & Carapezza, M. L. The Problem of Volcanic Unrest: The Campi Flegrei Case History. in *Monitoring and Mitigation of Volcano Hazards* 771–786 (Springer Berlin Heidelberg, 1996). doi:10.1007/978-3-642-80087-0_23.

12. Hicks, A. & Few, R. Trajectories of social vulnerability during the Soufrière Hills volcanic crisis. *J. Appl. Volcanol.* **4**, 10 (2015).

13. Kilburn, C. R. J., De Natale, G. & Carlino, S. Progressive approach to eruption at Campi Flegrei caldera in southern Italy. *Nat. Commun.* **8**, 1–8 (2017).

14. Brown, S. K., Sparks, R. S. J. & Jenkins, S. F. Global distribution of volcanic threat. in *Global Volcanic Hazards and Risk* (eds. Loughlin, S. C., Sparks, S., Brown, S. K., Jenkins, S. F. & Vye-Brown, C.) 359–369 (Cambridge University Press, 2015). doi:10.1017/CBO9781316276273.025.

15. De Natale, G., Pingue, F., Allard, P. & Zollo, A. Geophysical and geochemical modelling of the 1982-1984 unrest phenomena at Campi Flegrei caldera (southern Italy). *J. Volcanol. Geotherm. Res.* **48**, 199–222 (1991).

16. De Siena, L. *et al.* Source and dynamics of a volcanic caldera unrest: Campi Flegrei, 1983-84. *Sci. Rep.* **7**, 1–13 (2017).

17. Orsi, G., D'Antonio, M., Vita, S. de & Gallo, G. The Neapolitan Yellow Tuff, a large-magnitude trachytic phreatoplinian eruption: eruptive dynamics, magma withdrawal and caldera collapse. *J. Volcanol. Geotherm. Res.* **53**, 275–287 (1992).

18. Deino, A. L., Orsi, G., de Vita, S. & Piochi, M. The age of the Neapolitan Yellow Tuff caldera-forming eruption (Campi Flegrei caldera – Italy) assessed by 40Ar/39Ar dating method. *J. Volcanol. Geotherm. Res.* **133**, 157–170 (2004).

19. Dvorak, J. J. & Berrino, G. Recent ground movement and seismic activity in Campi Flegrei, southern Italy: episodic growth of a resurgent dome. *J. Geophys. Res.* (1991) doi:10.1029/90JB02225.

20. Orsi, G., De Vita, S. & di Vito, M. The restless, resurgent Campi Flegrei nested caldera (Italy): constraints on its evolution and configuration. *J. Volcanol. Geotherm. Res.* **74**, 179–214 (1996).

21. De Natale, G. *et al.* The Campi Flegrei caldera: unrest mechanisms and hazards. *Geol. Soc. London, Spec. Publ.* **269**, 25–45 (2006).

22. Langella, A. *et al.* The Neapolitan Yellow Tuff: An outstanding example of heterogeneity. *Constr. Build. Mater.* (2017) doi:10.1016/j.conbuildmat.2017.01.053.

23. Moon, V. G. Geotechnical characteristics of ignimbrite: A soft pyroclastic rock type. *Eng. Geol.* **35**, 33–48 (1993).

24. Quane, S. L. & Russell, J. K. Rock strength as a metric of welding intensity in pyroclastic deposits. *Eur. J. Mineral.* **15**, 855–864 (2003).

25. Binal, A. Prediction of mechanical properties of non-welded and moderately welded ignimbrite using physical properties, ultrasonic pulse velocity, and point load index tests. *Q. J. Eng. Geol. Hydrogeol.* **42**, 107–122 (2009).

26. Fazio, M., Alparone, S., Benson, P. M., Cannata, A. & Vinciguerra, S. Genesis and mechanisms controlling tornillo seismo-volcanic events in volcanic areas. *Sci. Rep.* **9**, 1–11 (2019).

27. Kendrick, J. E. *et al.* Tracking the permeable porous network during strain-dependent magmatic flow. *J. Volcanol. Geotherm. Res.* **260**, 117–126 (2013).

28. Burlini, L. *et al.* Seismicity preceding volcanic eruptions: New experimental insights. *Geology* **35**, 183–186 (2007).

29. Main, I. Earthquake scaling. *Nature* vol. 357 27–28 (1992).

30. Hatton, C. G., Main, I. G. & Meredith, P. G. A comparison of seismic and structural measurements of scaling exponents during tensile subcritical crack growth. *J. Struct. Geol.* **15**, 1485–1495 (1993).

31. Aki, K. & Koyanagi, R. Deep volcanic tremor and magma ascent mechanism under Kilauea, Hawaii. *J. Geophys. Res.* (1981) doi:10.1029/JB086iB08p07095.

32. Burlini, L. *et al.* Seismicity preceding volcanic eruptions: New experimental insights. *Geology* **35**, 183–186 (2007).

33. Benson, P. M., Thompson, B. D., Meredith, P. G., Vinciguerra, S. & Young, R. P. Imaging slow

failure in triaxially deformed Etna basalt using 3D acoustic-emission location and X-ray computed tomography. *Geophys. Res. Lett.* **34**, 1–5 (2007).

34. Fazio, M., Benson, P. M. & Vinciguerra, S. On the generation mechanisms of fluid-driven seismic signals related to volcano-tectonics. *Geophys. Res. Lett.* **44**, 734–742 (2017).

35. Heap, M. J. *et al.* The influence of water on the strength of Neapolitan Yellow Tuff, the most widely used building stone in Naples (Italy). *Bull. Volcanol.* (2018) doi:10.1007/s00445-018-1225-1.

36. Townend, E. *et al.* Imaging compaction band propagation in Diemelstadt sandstone using acoustic emission locations. *Geophys. Res. Lett.* **35**, 1–5 (2008).

37. Smith, R., Sammonds, P. R. & Kilburn, C. R. J. Fracturing of volcanic systems: Experimental insights into pre-eruptive conditions. *Earth Planet. Sci. Lett.* **280**, 211–219 (2009).

38. Lockner, D. A., Byerlee, J. D., Kuksenko, V., Ponomarev, A. & Sidorin, A. Quasi-static fault growth and shear fracture energy in granite. *Nature* **350**, 39–42 (1991).

39. Thompson, B. D. Observations of premonitory acoustic emission and slip nucleation during a stick slip experiment in smooth faulted Westerly granite. *Geophys. Res. Lett.* **32**, L10304 (2005).

40. Harnett, C. E., Benson, P. M., Rowley, P. & Fazio, M. Fracture and damage localization in volcanic edifice rocks from El Hierro, Stromboli and Tenerife. *Sci. Rep.* **8**, 1942 (2018).

41. Benson, P. M., Vinciguerra, S., Meredith, P. G. & Young, R. P. Spatio-temporal evolution of volcano seismicity: A laboratory study. *Earth Planet. Sci. Lett.* **297**, 315–323 (2010).

42. Clarke, J. *et al.* The relation between viscosity and acoustic emissions as a laboratory analogue for volcano seismicity. *Geology* **47**, 499–503 (2019).

43. Bean, C. J. *et al.* Long-period seismicity in the shallow volcanic edifice formed from slow-rupture earthquakes. *Nat. Geosci.* **7**, 71–75 (2014).

44. Neuberg, J., Luckett, R., Baptie, B. & Olsen, K. Models of tremor and low-frequency earthquake swarms on Montserrat. *J. Volcanol. Geotherm. Res.* **101**, 83–104 (2000).

45. Massonnet, D. & Feigl, K. L. Radar interferometry and its application to changes in the earth's surface. *Rev. Geophys.* **36**, 441–500 (1998).

46. Barberi, F. *et al.* The campanian ignimbrite: a major prehistoric eruption in the Neapolitan area (Italy). *Bull. Volcanol.* (1978) doi:10.1007/BF02597680.

47. Scarpati, C., Cole, P. & Perrotta, A. The Neapolitan Yellow Tuff ? A large volume multiphase eruption from Campi Flegrei, Southern Italy. *Bull. Volcanol.* **55**, 343–356 (1993).

48. Benson, P. M. *et al.* Laboratory simulations of fluid-induced seismicity, hydraulic fracture, and fluid flow. *Geomech. Energy Environ.* 100169 (2020) doi:10.1016/j.gete.2019.100169.

49. Fairhurst, C. E. ; Hudson, J. A. Draft ISRM suggested method for the complete stress-strain curve for intact rock in uniaxial compression. *Int. J. Rock Mech. Min. Sci.* **36**, 279–289 (1999).